Self-feeding paper based biofuel cell/self-powered hybrid μ-supercapacitor integrated system

Self-Feeding Paper Based Biofuel Cell / Self-Powered hybrid μ-supercapacitor integrated system

Claudia W. Narvaez Villarrubia[1,a], *Francesca Soavi[2,a], Carlo Santoro[3,a], Catia Arbizzani[2], Alexey Serov[3], Santiago Rojas-Carbonell[3], Gautam Gupta[1], **Plamen Atanassov[3].

[1] MPA-11 Material Synthesis and Integrated Devices, Los Alamos National Laboratory, Los Alamos, NM, USA

[2] Department of Chemistry "Giacomo Ciamician", Alma Mater Studiorum - Università di Bologna, Via Selmi, 2, 40126 Bologna, Italy

[3] Center Micro-Engineered Materials (CMEM), Department of Chemical and Biological Engineering, University of New Mexico, NM, USA

[a] the three authors have contributed equally to the manuscript

***corresponding authors**

* Francesca Soavi, Department of Chemistry "Giacomo Ciamician", Alma Mater Studiorum-Università di Bologna, Via Selmi, 2, Bologna, Italy, e-mail: francesca.soavi@unibo.it

** Plamen Atanassov, Center for Micro-Engineered Materials (CMEM), Department of Chemical & Biological Engineering, University of New Mexico, Albuquerque, NM 87131, USA, e-mail: plamen@unm.edu

Abstract

For the first time, a paper based enzymatic fuel cell is used as self-recharged supercapacitor. In this supercapacitive enzymatic fuel cell (SC-EFC), the supercapacitive features of the electrodes are exploited to demonstrate high power output under pulse operation. Glucose dehydrogenase-based anode and bilirubin oxidase-based cathode were assembled to a quasi-2D capillary-driven microfluidic system. Capillary flow guarantees the continuous supply of glucose, cofactor and electrolytes to the anodic enzyme and the gas-diffusional cathode design provides the passive supply of oxygen to the catalytic layer of the electrode. The paper-based cell was self-recharged under rest and discharged by high current pulses up to 4 mA cm^{-2}. The supercapacitive behavior and low equivalent series resistance of the cell permitted to achieve up to a maximum power of 0.87 $mWcm^{-2}$ (10.6 mW) for pulses of 0.01 s at 4 mA cm^{-2}. This operation mode allowed the system to achieve at least one order of magnitude higher current/power generation compared to the steady state operation. Three days durability tests (4200 cycles) were run at current pulses of 0.4 $mAcm^{-2}$. Results showed a slight decrease in working open circuit voltage (OCV) and a decrease of cell capacitance during the operations.

Keywords: Enzymatic Fuel Cell, Supercapacitor, paper-based microfluidic system, power pulses

1. Introduction

Enzymatic fuel cells (EFC) are energy and power harvesting devices, theoretically, capable to obtain high power density from biofuels at circum-neutral pH. However, actual power and energy density is lower than theoretical performance (Minteer et al., 2007; Davis et al.; 2007; Yu and Scott, 2010; Falk et al., 2013; Cosnier et al., 2014; Slaughter et al. 2015). Optimum power/energy harvesting still remains a challenge to overcome when compared to commercial batteries and conventional fuel cells (FCs). Consequently, an improved internal design and its integration with other electrochemical devices such as a supercapacitor seems to be appropriate for enhancing the performance up to the level required to power small portable devices or biomedical devices (Southcott el at., 2013, Narváez Villarrubia et al., 2014; Pankratov et al., 2016; Kizling et al., 2015).

Redox enzymes are employed for enzymatic fuel cell (EFC) applications to harvest energy from biofuels found in nature (Minteer et al., 2007; Davis et al.; 2007; Yu and Scott, 2010; Falk et al., 2013; Cosnier et al., 2014). These enzymes are specific for catalyzing the reduction or oxidation of their substrates, offering a high theoretical efficiency, leaving no toxic residues of reaction (Sokic-Lazic et al., 2008; Gellett et al., 2010; González-Guerrero et al.; 2013; Tam et al., 2009; Amir et al., 2009). Enzymatic fuel cells offer the capability to operate at room temperature and neutral pH, conditions which cannot be achieved by conventional FCs (Heller, 1992; Mano et al., 2003; Soukharev et al., 2004; Kang et al.,

2006). Even though these devices provide several advantages, the effect of various limiting factors on the system result in low power output generation. Stability of the enzymes outside their natural environment, the partial oxidation of the substrates and transport of biofuels to the catalytic sites of the electrodes are factors limiting the performance of EFCs. Certain criteria to mitigate the limiting factors mentioned above need to be satisfied to improve efficiency (Pardo-Yissar et al., 2000; Tarasevich et al., 2002; Moore et al., 2005; Atanassov et al., 2007; Cooney et al., 2008; Ivnitski et al., 2008; Gupta et al., 2009; Rincon et al., 2011; Minteer, 2012a; Minteer et al., 2012b; Reid et al., 2013; Rasmussen et al. 2016). In Addition, the need of an efficient transport of fuel to the catalytic sites should be addressed.

Our group addressed those issues, in previous research, constructing a biodegradable EFC that independently powered a small device for 36 hours (Ciniciato et al., 2012; Narvaez Villarrubia et al., 2014) and, later, used an enzymatic cascade system working with ethanol and methanol (Lau et al., 2015). The catalytic layer was designed to enhance enzyme loading and stability using a highly porous and conductive bucky-paper (multiwall carbon nanotubes (MWCNTs)-based paper). Also, a cellulose paper-based quasi-2D microfluidic system was utilized to self-transport fuel to the catalytic layer on the electrodes as well as to work as proton exchange membrane, electrode separator and structural mechanical support. This self-fed EFC design offered the possibility to power small devices utilizing ubiquitous fuels, and simultaneously addressing environmental concerns. Assembling this EFC to a supercapacitor could enhance its performance to achieve energy/power demand of small devices for various applications. Several studies have shown paper-based systems feasibly used to develop bioelectrodes and microfluidic

systems mainly for biosensors or EFC to power biosensors (Shitanda et al. 2013; Strack et al. 2013; Li et al. 2015; Reid et al. 2015; Slaughter et al. 2016; Majdecka et al. 2016; Desmet et al. 2016). Powering small portable or medical devices that demand higher energy/power is a challenge to overcome by designing hybrid systems.

Supercapacitors are high power electrochemical energy storage systems with high capacitance electrodes that can be charged and discharged through fast and reversible processes (Beguin et al.; 2014; Conway, 1999). They are considered the most suitable devices for high power pulse delivery. Examples of hybrid bio-devices integrating supercapacitors such as bio-batteries and biosensors, utilizing enzymatic systems, were developed by Skunik-Nuckowska *et al*. (2014) and Kizling *et al.* (2015), respectively. The integration of internal supercapacitors within biofuel cells has been shown in previous studies by Pankratov *et al.* (2014a; 2014b; 2014c), by González-Arribas *et al.* (2016) and by Agnes *et al*. (2014).

Pankratov *et al.* have developed, for the first time, a self-charging bio-capacitor using cellobiose dehydrogenase (CDH) and bilirubin oxidase (BOx) as anodic and enzymatic systems, respectively, where the electrochemical capacitor and the EFC function simultaneously (Pankratov *et al.* 2014a; 2014c). Higher power pulses were obtained by Agnès *et al*. (2014). They used glucose oxidase (GOx) and catalase enzymes at the anode and laccase at cathode, correspondingly. Both anodic and cathodic enzymatic systems were entrapped in carbon nanotubes (CNTs)-based matrix conforming pellet-like bio-electrodes. The bio-electrodes were immerged into an electrolytic solution containing glucose and oxygen that was actively supplied by a pump (air saturated solution). The open circuit potential was roughly 800 mV with a total equivalent series resistance (ESR) of 37 Ω and

113 the highest power recorded of 18 mW (Agnès et al., 2014). These systems show to be
114 dependent of external biofuel and oxygen supply and their configuration are similar to bio-
115 batteries (functioning in a static electrolytic cell).

116 Hanashi et al. (2009) and Sode et al. (2016) revisited the challenges of biofuel cell
117 exploiting the possibility of combining charge pumps and capacitors in order to create a
118 stand-alone self-powered bio-device. In parallel, in recent research on microbial fuel cells
119 Santoro et al. developed an internal supercapacitor using the electrode reactions to develop
120 electrostatically self-rechargeable bioelectrodes (Santoro et al., 2016a, Soavi et al., 2016).

121 Herein, for the first time, a self-fed paper-based biofuel cell integrated at materials
122 level within an internal self-powered supercapacitor is reported. The glucose
123 dehydrogenase (GDH) enzymatic anode and BOx enzymatic cathode are used as
124 supercapacitors bio-electrodes and galvanostatic discharges are performed at currents that
125 are one order of magnitude higher than what is typical for standard operation of biofuel
126 cells. In open circuit conditions, the EFC stacking is analogous to that of a charged aqueous
127 electrochemical double layer capacitor (EDLC) that can be electrostatically discharged at
128 high current rates and, then, self-recharged by resetting cell in rest, demonstrating the proof
129 of concept for enzymatic electrodes using quasi-2D microfluidic system. The results of the
130 galvanostatic test performed in depletion mode and at different pulse times with currents
131 ranging between 0.4 mA cm^{-2} and 4 mA cm^{-2} are reported and discussed. Durability tests
132 for 4200 discharge/self-recharge cycles over a period of 72 hours (3 days) are also
133 presented.

134 This design opens the possibilities for the development of self-sustained
135 environmentally friendly hybrid EFCs-supercapacitors (SC-EFC) that can feasibly be used

for practical applications, which demand different ranges of power/current density, and duration of operation such as sensors, *ex-vivo* biomedical devices or other portable devices, with an autonomy not envisioned before.

2. Materials and Methods

2.1 Bio-electrodes Fabrication and Device Assembly

The paper-based biofuel cell was composed by an anode based on glucose dehydrogenase (GDH) enzyme and by a cathode based on BOx as previously presented (Ciniciato et al., 2012; Narvaez Villarrubia et al., 2014). On one hand, the cathode was a dual-layered passive-gas diffusional electrode constituted of a hydrophobic layer that promoted the flow of oxygen to the catalytic sites and a catalytic layer conformed by the enzymatic system (schematic shown in figure 1.A). Toray paper (TP) was used as current collector. On top of it, the hydrophobic layer was pressed, which consisted of Vulcan XC72 carbon black that was teflonized to a 35wt% and is referred as XC35. The loading of this teflonized carbon over the TP-current collector was 83±1 mg cm^{-2} and 263 psi of pressure was applied for 10 minutes to assemble the hydrophobic layer (TP-XC35 pellet). After the pellet was formed, 10 μLcm^{-2} of isopropanol were added in order to increase the hydrophobic/hydrophilic gradient within the TP-XC35 and increase the oxygen "breathing" from the atmospheric environment to the catalytic layer (Narvaez Villarrubia et al., 2014; Santoro et al., 2016b). Subsequently, buckypaper (20 gsm C-Grade MWCNTs based-paper with BET area of 33 $m^2 g^{-1}$) was pressed on top of the pellet, for additional 5

159 minutes at the same pressure (263 psi) to form the catalytic layer were BOx was deposited.
160 For this, 80 mg of BOx enzyme was dissolved in 1 ml of phosphate buffer saline (PBS)
161 0.1M at pH 7.5 and deposited over night (~12 hours) on the electrode at 4 ºC (Santoro et
162 al., 2016b). The electrode had dimensions of 3.5 cm x 3.5 cm (12.25 cm^2) and the loading
163 of the buckypaper was roughly 2 mg cm^{-2}. Further optimization of the immobilization
164 process of the enzyme and the fabrication of high performing gas diffusional electrodes
165 has been proposed (Rojas-Carbonell et. al., 2016).

166 The anode was prepared utilizing nicotinamide adenine dinucleotide
167 (NAD^+/NADH) dependent GDH enzyme (schematic shown in figure 1.B). The electrode
168 consisted of a bucky paper piece (20gsm C-grade MWNTs based-paper with BET area of
169 33 m^2g^{-1}) with rectangular shape of also 12.25 cm^2 (3.5 cm x 3.5 cm) with a 'tail' of 2 cm
170 length and 1.5 cm width that served as contact to the external circuit. Also in this case, the
171 buckypaper loading was similar compared to the one used for the cathode (roughly 2 mg
172 cm^{-2}).

173 Methylene green (MG), a mediator for NADH oxidation to NAD^+, was
174 electrodeposited as previous research procedure stated (Narváez Villarrubia et al., 2011;
175 2013; Svobova et al. 2007). Later, 9.93 mg of GDH was dissolved in 496 µl of 95%
176 Chitosan / 5% MWCNTs and deposited on the electrode overnight (~12 hours) at 4ºC
177 (Narváez Villarrubia et al., 2013, 2014; Svobova et al. 2007). Even though this anode uses
178 cofactor and mediator to function, its structural design generates higher current densities
179 when compared to GOx (Narváez Villarrubia et al., 2011; 2013; 2014,).

180 The bio-electrodes were assembled to a quasi-2D capillary-driven microfluidic
181 system (Mendez et al., 2010; Benner and Petsev, 2013). This was a 'fan'-shaped paper-

182 based system, introduced in our previous research (Narváez Villarrubia et al., 2014),
183 consisting of a 3.5 cm × 3.5 cm rectangle appended to a 180°-circular section of 24 cm of
184 diameter (Grade 1 Whatman filter paper). Both bio-electrodes, placed with the catalytic
185 layers facing the paper, were stacked on the rectangular section of the paper-'fan' (Figure
186 1). The biocathode was placed on the microfluidic system assuring an aperture for passive
187 oxygen diffusion from air. Similarly to our previous research, the device was immersed in
188 an electrolytic solution of glucose 0.1M NAD^+ 1mM and 0.1M KCl dissolved in PBS 0.1M
189 at pH 7.5.
190
191 **2.2 Hybrid Paper-Based EFC-Supercapacitor Characterization**
192 Electrochemical tests were performed on the SC-EFC using a potentiostat (SP-50, Bio-
193 Logic, France). The capacitive response of the single electrodes and the overall biofuel cell
194 was investigated utilizing cyclic voltammetry (CV) in two- and three- electrode modes. In
195 the latter case, Ag/AgCl (3M KCl) was used as reference electrode and placed in the
196 electrolyte reservoir. Cathode CVs were run by using the cathode as the working electrode
197 and the anode as counter electrode. For the anode CVs, the cathode was employed as
198 counter electrode. This permitted to get the voltammetric response of the single electrodes
199 in-situ, i.e. in the paper-based biofuel cell setup. Anode and cathode CVs were run between
200 -0.2 V and 0.2 V (vs Ag/AgCl 3M KCl) and 0 V to 0.5 V (vs Ag/AgCl 3M KCl),
201 respectively. Cell CVs were run between 0 and 0.6 V in 2-electrode mode with the cathode
202 being the working electrode and the anode the reference and counterelectrode. In the latter
203 case, cell CVs were also carried out with identical electrodes not loaded with enzymes as
204 a control.

All the CVs were run at scan rate of 5 and 50 mVs^{-1}. Energy and power performances of the enzymatic fuel cell were evaluated by analysis of the cell voltage profiles under galvanostatic discharge (GLV). GLV discharges of the SC-EFC were performed from OCV to 0 V at different current densities (i_{pulse}) varying from 0.4 mA cm^{-2} to 4 mA cm^{-2}. Ag/AgCl reference electrode was used to monitor the anode and cathode potentials during discharge. The GLV discharge causes the decrease of the open circuit voltage of the charged cell ($V_{max,\ oc}$) by an ohmic drop (ΔV_{ohmic}) that is related to the equivalent series resistance (ESR) of the SC-EFC, to which contribute electrolyte and electrodes resistances. The ESR is calculated as the ratio between the ΔV_{ohmic} and the pulse current applied (i_{pulse}). Following the ohmic drop, a capacitive decrease of the voltage over time ($\Delta V_{capacitive}$) takes place due to the kinetics of the redox processes and to the capacitive features of the SC-EFC electrodes. The cell and electrode capacitances (C) were calculated from the ratio between i_{pulse} and the slope (s) in the cell voltage (or electrode potential)-time curve. Practical values of maximum energy (E_{max}) and power (P_{max}) were evaluated considering the maximum available voltage after the ohmic drop (V_{max}) calculated as the difference between the open circuit voltage (OCV) of the charged cell ($V_{max,\ oc}$) and ΔV_{ohmic}. P_{max} was obtained multiplying i_{pulse} and V_{max}. As discussed above, the voltage decreases over the discharge pulse, along with the practical energy, E_{pulse}, which is delivered during the pulse and which is calculated by the following equation:

$$E_{pulse} = i_{pulse} \int_0^{t_{pulse}} V\ dt \quad (1)$$

where t_{pulse} is the pulse time.

The pulse power (P_{pulse}) is lower than P_{max} and corresponds to $P_{pulse,} = E_{pulse,} / t_{pulse}$, (2)

PLEASE INSERT HERE FIGURE 1

3. Results and discussion

3.1 Voltammetric Survey

PLEASE INSERT HERE FIGURE 2

Figure 2.a compares the voltammogramms of the cell with the presence and the absence of enzymes at 5 mV s^{-1} and 50 mV s^{-1}. At the highest scan rate, the two cells feature almost the same cathodic currents, therefore unraveling a similar capacitive behaviour. A capacitance of 5.4 mF cm^{-2} (65 mF) is deduced for both systems dividing the current density by the scan rate. The main difference between the two cells is evident in the anodic currents. The enzyme loaded cell exhibits lower currents than the cell without enzymes. The voltammogram of the former cell deviates from the symmetric box shaped one that is expected for supercapacitors assembled with high surface area carbon electrodes, and which in turn is obtained with the no-enzyme cell. Such different behaviour is further evidenced at the lowest scan rate (Figure 2.a). At 5 mV s^{-1}, the faradic and irreversible processes that characterize the biofuel cell operation, namely glucose oxidation and oxygen reduction, are driving the CV response of the cell. In order to investigate the contribution of each electrode to the overall cell response, CVs were performed in 3-electrode mode

and the results at 50 mV s^{-1} are shown in Figure 2.b. Cathode response is almost symmetric with currents similar to those featured by the cell. This indicates that cell capacitive response is dominated by the cathode. In turn, the anode CVs are distorted and above 0.1 V vs Ag/AgCl 3M KCl, a steep increase of the anodic current can be appreciated due to the onset of glucose oxidation.

Figure 2 indicates that at the highest scan rates (and currents), the main contribution to the cell capacitance is given by the electric double layer formed at the carbonaceous electrodes interfaces. At the lowest scan rates (and currents), the enzymatic faradic processes, and specifically ORR, are playing the major role and increase cell capacitance with respect to the cell without enzymes. The main difference between the cell with and without enzyme is that, in rest conditions, the open circuit voltage (OCV) of the cell with no enzymes is around 0 V because it is assembled with identical electrodes experiencing the same electrolyte with identical environments. The presence of enzymes allowed the cell to feature an OCV of roughly 600 mV due to the different equilibrium potentials of the redox processes taking place at the anode and cathode. Consequently, this enables the self-polarization of the electrodes that can be exploited to design the supercapacitive self-powered biofuel cell that is dicussed in the further sections.

3.2 Overall and single electrode discharge profiles

PLEASE INSERT HERE FIGURE 3

Cell voltage and electrodes potential profiles of the SC-EFC under a discharge at 0.4 mA cm^{-2} (i_{pulse} of 5 mA) and the following self-recharge is presented in Figure 3.a. Cell voltage and electrodes potential profiles of the SC-EFC under discharges at different currents and the following self-recharge are presented in Figure S1. The open circuit voltage of the paper based biofuel cell was 563±14mV in agreement with previously presented data. The cathode open circuit potential (OCP) was +496±4 mV vs Ag/AgCl (the positive electrode) and anode OCP was -66±13 mV vs Ag/AgCl (the negative electrode). These values agree with previously reported OCP for glucose dehydrogenase and bilirubin oxidase (Narváez Villarrubia et al., 2013; 2014).

The cell voltage linearly decreases during the pulse like in EDLCs. From the slope of the cell voltage over time at i_{pulse} of 0.4 mA cm^{-2} a cell capacitance value of 8.25 mF cm^{-2} is obtained. The profiles of the electrodes potentials evidence that cell capacitance is mainly affected by the positive electrode response. Indeed, while the positive electrode potential linearly decreases during discharge and exhibits 9.4 mF cm^{-2}, the negative electrode potential increase during the discharge is almost negligible. The positive electrode capacitance is reasonably low because of the low surface area (33 $m^2 g^{-1}$) and low carbon loading (2 mg cm^{-2}) of the buckypaper. On the other hand, the capacitive response of the negative electrode, with exactly the same surface area and loading of the positive electrode, is much higher and was measured as 67 mF cm^{-2}.

This suggests that while during discharge the positive electrode behaved like a conventional EDLC positive electrode, the negative electrode responded by a fast redox process, namely the oxidation of glucose by the enzymatic process. Hence, at such high current response, the SC-EFC operates like a hybrid supercapacitor, i.e. a capacitor with a

296 positive electrode working by an electrostatic process and a negative electrode working by
297 a Faradic process. Note that, this is highlighted by the anode CV reported in Figure 2b, in
298 which glucose oxidation is not reversible. Therefore, for sake of clarity, we would like to
299 underline that the negative electrode cannot be termed "pseudocapacitive" as it would be
300 in a conventional hybrid supercapacitor.

301 At 0.4 mA cm^{-2} the full discharge time was ≈9.1 s followed by a ≈16 s recharge
302 obtained without the utilization of any external device (Figure 3.a). Indeed, during the rest
303 period in open circuit after the pulse, electrode potentials moved back to their initial
304 equilibrium values and cell voltage was restored to the value exhibited before the pulse.
305 The EFC was, then, tested at higher current densities (0.8 to 4 mA cm^{-2}), and the cell
306 voltage (Figure 3.b) and electrodes potential (Figure 3.c) profiles for i_{pulse} ranging from 0.8
307 mA cm^{-2} to 4 mAcm^{-2} are reported.

308 As expected, the discharge time decreased with the increase of the i_{pulse}. The
309 complete discharge of the supercapacitor took place in ≈9.1 sec at 0.4 mA cm^{-2} (Figure 3.a)
310 and 0.053 sec at 4 mA cm^{-2} applied (Figure 3.b). Cell voltage profiles were shaped by the
311 different rate response of positive and negative electrode. The positive electrode potential
312 profiles were mainly affected by electrode capacitive behavior while the negative electrode
313 potential profiles were mainly affected by the ohmic drop, i.e. by negative electrode
314 resistance. In fact, the overall ESR was 6 Ω (0.49 Ω cm^2) in which 4 Ω (0.33 Ω cm^2) and 2
315 Ω (0.16 Ω cm^2) were due to negative electrode and positive electrode respectively. Indeed,
316 at the lowest current investigated (0.4 mA cm^{-2}), the positive electrode ohmic drop was
317 only of ≈10 mV, to be compared to ≈20 mV for the negative electrode (Figure 3.a). During
318 the complete discharge, the voltage decrease of the positive electrode was ≈478 mV, much

higher compared to the voltage decrease of the negative electrode ≈77 mV. At the highest current investigated (4 mA cm^{-2}), the positive electrode ohmic drop was only of ≈100 mV, to be compared to ≈200 mV for the negative electrode. The voltage decrease of the positive electrode during the pulse (4 mA cm^{-2}) was ≈160 mV and much higher than that of the negative electrode (≈40 mV). Hence, ΔV_{ohmic} of the cell was mainly affected by the negative electrode (which mainly contributes to cell ESR) while the $\Delta V_{capacitive}$ of the cell was mainly affected by the positive electrode.

Additionally, negative electrode and positive electrode contribute differently to cell response under short and long-time pulses. At short time (10 ms) pulses, the cell performance is mainly affected by the ohmic drop, which in turn mainly depends on the negative electrode. Instead, at longer times, cell performance is influenced by the capacitive response of the positive electrode.

The curves reported in Figure 3 were used to evaluate cell performance at very short and at longer time pulse response. The maximum power is calculated on the basis of the cell ESR and does not consider the capacitive behavior, hence it is representative of the short time response of the cell. E_{pulse} and P_{pulse} are calculated considering the complete discharge profile over the entire pulse duration. Thus, they represent the practical cell performance at different time pulses and pulse currents.

3.3 Power Curves and Ragone Plot

PLEASE INSERT HERE FIGURE 4

342

343 P_{max} was calculated at different current densities considering V_{max} of 0.56 V and
344 ESR of 6 Ω (Figure 4.a). The highest value of 1.07 mW cm^{-2} (13.1 mW) was measured for
345 current pulse of 3.6 mA cm^{-2}. This value is one order of magnitude higher than the power
346 obtained by the biofuel cell in stationary operation (Narváez Villarrubia et al., 2014).
347 Figure 4.a also reports the P_{pulse} for different t_{pulse} of 1, 0.5, 0.25, 0.1 and 0.01 sec at
348 different currents. As expected, P_{pulse} decreases with the increase of time due to the
349 capacitive response of the cell which decreases the cell voltage over time. The highest value
350 of P_{pulse} was 0.27 mW cm^{-2} for t_{pulse} of 1 s, 0.387 mW cm^{-2} for t_{pulse} of 0.5 s, 0.509 mW cm^{-2}
351 at t_{pulse} for 0.25 s, 0.66 mW cm^{-2} for t_{pulse} of 0.1 s, and 0.868 mW cm^{-2} for t_{pulse} of 0.01 s.

352 The values of E_{pulse} and P_{pulse}, for complete discharges, from $V_{max,OC}$ to 0V, at
353 different currents were used to build the Ragone plot reported in Figure 4.b. The highest is
354 the current, the lower is E_{pulse} and the highest is P_{pulse}.

355 The highest energy and power densities for complete discharges are 0.177 μWh cm^{-2}
356 (0.4 mA cm^2, 9.015 s) and 393 μW cm^{-2} (3.2 mA cm^{-2}, 0.141 s) respectively. Complete
357 discharges of ca. 0.5 s (1-2 mA cm^{-2}) provide the best matching for P_{pulse} (200-300 μW cm^{-2})
358 and E_{pulse} (0.04-0.05 μWh cm^{-2}).

359 Durability tests over 3 days (4200 cycles) have been conducted and presented in
360 the supporting information [Figure S2]. The results indicated a slight decrease in working
361 open circuit voltage (OCV) and cell capacitance over time [Figure S2].

362

363 **3.5 Outlook**

364

For the first time, a self-fed paper based biofuel cell was used as hybrid self-powered μ-supercapacitor which delivers significant power under short and high current pulses compared to conventional EFC operation. In this case, positive electrode responded using an electrostatic process while the negative electrode worked using a Faradic process like in a hybrid supercapacitor. The particular configuration of EFC allows a continuous and constant biofuel supply through capillary-driven flow, electrolytes and products of reaction through the quasi-2D microfluidic system. Differently to previous studies (Pankratov et al. 2014a; 2014b; 2014c; Agnes et al., 2014), in this research oxygen was not actively supplied in the electrolyte. Furthermore, electrolyte was wetting electrode exploiting capillarity, which might explain the lower cathode capacitive performances registered. In fact, the passive diffusion of oxygen from air to the three phase interface of the catalytic layer of the cathode is driven by a concentration gradient in the hydrophilic/hydrophobic layers formed with the specific configuration of this biocathode. High capacitive response requires that the high surface area of the carbon is entirely wetted with the electrolytic solution. The main advantage of the paper-based biofuel cell / supercapacitor integrated system lays in the fact that this system is self-powered and self-sustained; it could work until complete depletion of biofuel, using no other external power source. This work demonstrates the feasibility of using selective enzymatic electrodes as electrochemical storage systems (i.e. supercapacitors) in a hybrid device that could work independently from external energy sources. Further studies should be completed in the utilization of amplified and pulsed signals into sensors development, or conformations to power *ex-vivo* biomedical devices or portable devices.

4. Conclusions

A glucose/air paper-based biofuel cell / supercapacitor integrated system was demonstrated with NAD^+/NADH-dependent glucose dehydrogenase and bilirubin oxidase enzymes employed at the anode and cathode, respectively. The paper-based microfluidic device allowed self-feeding of glucose (biofuel) and oxygen (oxidant) to the cell. The system has very low equivalent series resistance quantified in 6 Ω. The supercapacitive features of the electrodes generated short and high current pulse discharge up to 4 $mAcm^{-2}$. The practical power achieved was 1.07 mW cm^{-2} (13.1 mW), which is among the highest power ever recorded for this kind of hybrid systems. A maximum pulse power of 0.87 $mWcm^{-2}$ (10.64 mW) was measured for pulses of 0.01 s. The capacitive features of the nanostructured electrodes integrated in a 'fan' paper-based biofuel cell configuration enabled current and power densities at least one order of magnitude higher than compared to steady state mode. The SC-EFC cathode was limiting cell capacitance and improvements are expected by the use of a carbonaceous substrate of higher specific surface area. Utilization of carbon materials featuring at least 1000 $m^2\ g^{-1}$ could raise electrode response in the order of Farads, and increase pulse energy by 1-2 order of magnitude.

Acknowledgement

FS and CA acknowledge financial support by Alma Mater Studiorum - Università di Bologna (Researcher Mobility Program).

411 **References**

412

413 Agnès, C., Holzinger, M., Le Goff, A., Reuillard, B., Elouarzaki, K., Tingry, S., Cosnier
414 S., 2014. Energy Environ. Sci. 7, 1884-1888
415 Amir, L., Tam, T.K., Pita, M., Meijler, M.M., Alfonta, L., Katz, E., 2009. J. Am. Chem.
416 Soc. 131, 826-832.
417 Atanasov, P., Apblett, C., Brozik, S., Calabrese Barton, S.; Cooney, M., Liaw, B. Y.,
418 Mukerjee, S., Minteer, S. D. 2007. Electrochem. Soc. Interface. 16, 28–31.
419 Béguin, F., Presser, V., Balducci, A., Frackowiak, E., 2014. Adv. Mater. 26(14), 2219-
420 2251
421 Benner, E., Petsev, D.N., 2013. Potential flow in the presence of a sudden expansion:
422 Application to capillary driven transport in porous media. Phys. Rev. E 87 (033008),
423 1-10.
424 Ciniciato, G.P.M.K., Lau, C., Cochrane, A., Sibbett, S.S., Gonzalez, E.R., Atanassov, P.,
425 2012. Electroc. Acta 82, 208-213.
426 Conway, B.E., 1999. Electrochemical Supercapacitors: Scientific Fundamentals and
427 Technological Applications, Springer.
428 Cooney, M.J., Lau, C., Windmeisser, M., Liaw, B.Y., Klotzbach, T., Minteer, S.D., 2008.
429 J. Mater. Chem. 6, 667-674.
430 Cosnier, S., Holzinger, M., Le Goff, A.2008. Front. Bioeng. Biotechnol., 2(45), 1-5.
431 Davis, F., Higson, S.P.J., 2007. Biosens. Bioelectron. 22, 224-1235.
432 Desmet, C., Marquette, C. A., Blum, L. J., Doumèche, B., 2016. Biosen. Bioelectron. 76,
433 145–163.

Falk, M., Narvaez Villarrubia, C.W., Babanova, S., Atanassov, A., Shleev, S., 2013. ChemPhysChem 14(10), 2045-2058.

Garcia, S. O., Ulyanova, Y. V., Figueroa-Teran, R., Bhatt, K. H., Singhal, S., Atanassov, P., 2016. ECS J. Solid State Sci. Tech. 5 (8) M3075-M3081.

Gellett, W., Schumacher, J., Kesmez, M., Le, D., Minteer, S.D., 2010. J. Elechem. Soc. 157 (4), B557-B562.

González-Arribas, E., Pankratov, D., Gounel, S., Mano, N., Blum, Z., Shleev, S., 2016. Electroanalysis. doi: 10.1002/elan.201600096

González-Guerrero, M.J., Esquivel, J.P., Sánchez-Molas, D., Godignon, P., Xavier Muñoz, F., del Campo, F.J., Giroud, F., Minteer, S.D. Sabate, N., 2013. Lab Chip 13, 2972.

Gupta, G., Rathod, S.B., Staggs, K.W., Ista, L.K., Oucherif, K.A., Atanassov, P.B., Tartis, M.S., and Montano, G.A., Lopez, G.P., 2009. Langmuir 25(23), 13322-13327.

Hanashi, T., Yamazaki, T., Tsugawa, W., Ferri, S., Nakayama, D., Tomiyama, M., Ikebukuro, K., Sode, K., 2009. Biosens Bioelectron. 24, 1837-1842

Heller, A., 1992. J.Phys. Chem. 96, 3579-3587.

Ivnitski, D., Artyushkova, K., Rincón, R.A., Atanassov, P., Luckarift, H.R., Johnson, G.R., 2008. Small 4, 357-364.

Kang, C., Shin, H., Heller, A., 2006. Bioelectrochem. 68(1), 22-26.

Kizling, M., Draminska, S., Stolarczyk, K., Tammela, P., Wang, Z., Nyholm, L., Bilewicz, R., 2015. Bioelectrochem. 106, 34-40.

Lau, C., Moehlenbrock, M. J., Arechederra, R. L., Falase, A., Garcia, K., Rincon, R., Minteer, S. D., Banta, S., Gupta, G., Babanova, S., Atanassov, P. 2015. Int. J. Hydrogen Energy 40, 1461-1466.

457 Li, S., Wang, Y., Ge, S., Yu, S., Yan, M., 2015. Biosen. Bioelectron. 71, 18–24.
458 Majdecka, D., Bilewicz, R., 2016. J. Solid State Electrochem. 20, 949–955.
459 Mano, N., Mao, F., Shin, W., Chen, T., Heller, A., 2003. Chem. Comm, 518-519.
460 Mendez, S., Fenton, E.M., Gallegos, G.R., Petsev, D.N., Sibbett, S.S., Stone, H.A., Zhang,
461 Y., López, G.P., 2010. Langmuir 26, 1380-1385.
462 Minteer, S.D., Liaw, B.Y., Cooney, M.J., 2007. Curr. Opin. Biotech. 18, 228 - 234.
463 Minteer, S.D., 2012a. Top. Catal. 55, 1157-1161.
464 Minteer, S.D., Atanassov, P., Luckarift, H.R., Johnson, G.R., 2012b. Mater. Today 15(4),
465 166-173.
466 Moore, C.M., Minteer, S.D., Martin, R.S., 2005. Lab Chip 5, 218-225.
467 Narváez Villarrubia, C.W., Rincon, R.A., Radhakrishnan, V.K.; Davis, V., Atanassov, P.,
468 2011. ACS App. Mater. Interfaces 3, 2402-2409.
469 Narváez Villarrubia, C.W., Garcia, S.O., Lau, C., Atanassov, P., 2013. ECS J. Solid State
470 Sci. Technol. 2(10), M3156-M3159.
471 Narváez Villarrubia, C.W., Lau, C., Ciniciato, G.P.M.K., Garcia, S.O., Sibbett, S.S.,
472 Petsev, D.N., Babanova, S., Gupta, G., Atanassov, P., 2014. Electrochem. Comm. 45,
473 44-47.
474 Pardo-Yissar, V., Katz, E., Willner, I., Kotlyar, A.B., Sanders, C., Lill, H., 2000. Farad.
475 Discuss. 116, 119-134.
476 Pankratov, D., Blum, Z., Shleev, S., 2014a. ChemElectroChem 1, 1798 - 1807.
477 Pankratov, D., Falkman, P., Blum, Z., Shleev, S. Energy Environ. Sci. 2014b, 7, 989-993.
478 Pankratov, D., Blum, Z., Suyatin, D.B., Popov V.O., Shleev, S., 2014c. ChemElectroChem
479 1(2), 343-346.

480 Rasmussen, M., Abdellaoui, S., Minteer, S. D. 2016. Biosen. Bioelectron., 76, 91-102.
481 Reid, R.C., Giroud, F., Minteer, S.D., Galea, B.K., 2013. J. Electrochem. Soc. 160 (9),
482 H612-H619
483 Rincón, R.A., Lau, C., Garcia, K.A., Atanassov, P., 2011. Electrochim. Acta 56, 2503-
484 2509.
485 Rojas-Carbonell, S., Babanova, S., Serov, A., Ulyanova, Y., Singhal, S., Atanassov, P.,
486 2016. Electrochim. Acta, 190, 504-510.
487 Santoro, C., Soavi, F., Serov, A., Arbizzani, C., Atanassov, P., 2016a. Biosens.
488 Bioelectron. 78, 229-235
489 Santoro, C., Babanova, S., Erable, B., Schuler, A., Atanassov, P., 2016b. Bioelectrochem.
490 108, 1-7.
491 Shitanda, I., Kato, S., Hoshi, Y., Itagaki, M., Tsujimura, S., 2013. Chem. Commun. 49
492 (94), 11110–11112.
493 Skunik-Nuckowska, M., Grzejszczyk, K., Stolarczyk, K., Bilewicz R., Kulesza, P.J. 2014.
494 J. Appl. Electrochem. 44, 497-507.
495 Slaughter, G., Kulkarni, T., 2015. Biochip. Tissue Chip 5(1), 1-10.
496 Slaughter, G., Kulkarni, T., 2016. Biosen. Bioelectron. 78, 45-50.
497 Soavi, F., Bettini, L.G., Piseri, P., Milani, P., Santoro, C., Atanassov, P., Arbizzani, C.,
498 2016. J. Power Sources. doi:10.1016/j.jpowsour.2016.04.131
499 Sode, K., Yamazaki, T., Lee, I., Hanashi, T., Tsugawa, W., 2016. Biosens. Bioelectron. 76,
500 20–28.
501 Sokic-Lazic, D., Minteer, S.D., 2008. Biosensens. Bioelectron. 24, 939-944.
502 Soukharev, V., Mano, N., Heller, A., 2004. J. Am. Chem. Soc. 126(27), 8368-8369.

503 Southcott, M., MacVittie, K., Halámek, J., Halámková, L., Jemison, W. D., Lobel, R., Katz,
504 E., 2013. Phys.Chem.Chem.Phys. 15, 6278-6283.
505 Strack, G., Babanova, S., Farrington, K. E., Luckarift, H. R., Atanassov, P., Johnsona, G. R., 2013.
506 J. Electrochem, Soc. 160 (7), G3178-G3182.
507 Svoboda, V., Cooney, M.J., Rippolz, C., Liaw, B.Y., 2007. J. Electrochem. Soc. 154(3),
508 D113 - D116.
509 Tam, T.K., Pita, M., Ornatska, M., Katz, E., 2009. Bioelectrochem. 76(1-2), 4-9.
510 Tarasevich, M.R. Bogdanovskaya, V.A. Zagudaeva, N.M., Kapustin, A.V., 2002. Russ. J.
511 Electrochem. 38 (3), 335.
512 Yu, E.H., Scott, K., 2010. Energies 2010, 3, 23.

Figure Caption

Figure 1. A) Schematic of cathode fabrication, pressing process and BOx deposition. B) Schematic of anode fabrication, MG electrochemical deposition and GDH/Chitosan/CNTs mixture deposition. C) Paper-based EFC assembly, stacking of the cellulose paper-based microfluidic system. D) Paper-based SC-EFC using GDH and BOx as anode and cathode assembled to a quasi-2D microfluidic system inserted in a glucose 0.1M, 1 mM NAD^+ and KCl 0.1M in PB 0.1M at pH 7.5. E) Schematic of self-powered SC-EFC employing GDH anode and BOx cathode used as negative and positive electrodes of the internal supercapacitor, respectively.

Figure 2. Cell CVs with and without enzymes at scan rate of 5 mVs^{-1} and 50 mVs^{-1} (2-electrode mode) (a). Anode and cathode CVs at scan rate of 50 mVs^{-1} (b) (3-electrode-mode).

Figure 3. a) Cell voltage and electrodes potential profiles of the SC-EFC under a discharge at 0.4 mA cm^{-2} and the following rest period. b) Cell voltage and c) positive and negative electrode potential profiles during discharges at different current densities between 0.8 and 4 mA cm^{-2}.

Figure 4. a) Power curves at different current pulses. b) Ragone plot of the SC-EFC.

Figure 1

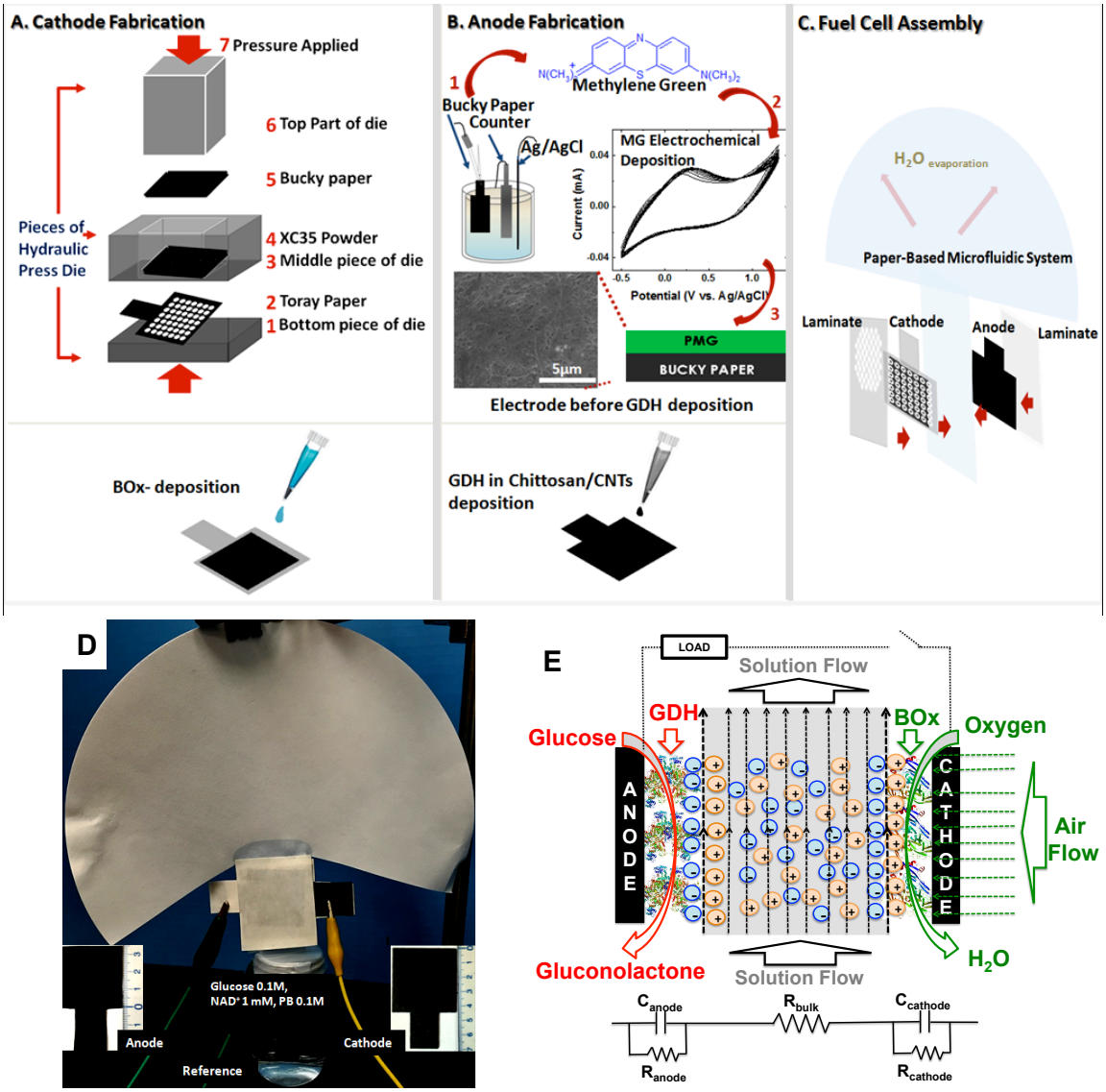
A. Cathode Fabrication
7 Pressure Applied
6 Top Part of die
5 Bucky paper
Pieces of Hydraulic Press Die
4 XC35 Powder
3 Middle piece of die
2 Toray Paper
1 Bottom piece of die
B. Anode Fabrication
Methylene Green
1
Bucky Paper Counter
Ag/AgCl
2
MG Electrochemical Deposition
Current (mA)
Potential (V vs. Ag/AgCl)
3
5µm
PMG
BUCKY PAPER
Electrode before GDH deposition
C. Fuel Cell Assembly
H2O evaporation
Paper-Based Microfluidic System
Laminate
Cathode
Anode
Laminate
BOx- deposition
GDH in Chittosan/CNTs deposition
D
Glucose 0.1M,
NAD+ 1 mM, PB 0.1M
Anode
Cathode
Reference
E
LOAD
Solution Flow
GDH
Glucose
BOx
Oxygen
ANODE
CATHODE
Air Flow
Gluconolactone
Solution Flow
H2O
Canode
Rbulk
Ccathode
Ranode
Rcathode

Figure 2

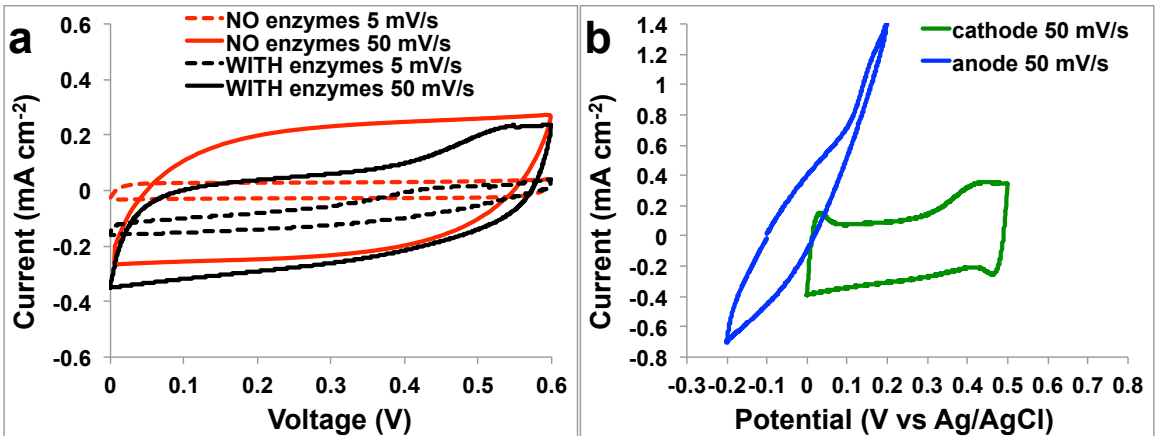
a
NO enzymes 5 mV/s
NO enzymes 50 mV/s
WITH enzymes 5 mV/s
WITH enzymes 50 mV/s
Current (mA cm-2)
Voltage (V)
b
cathode 50 mV/s
anode 50 mV/s
Current (mA cm-2)
Potential (V vs Ag/AgCl)

Figure 3

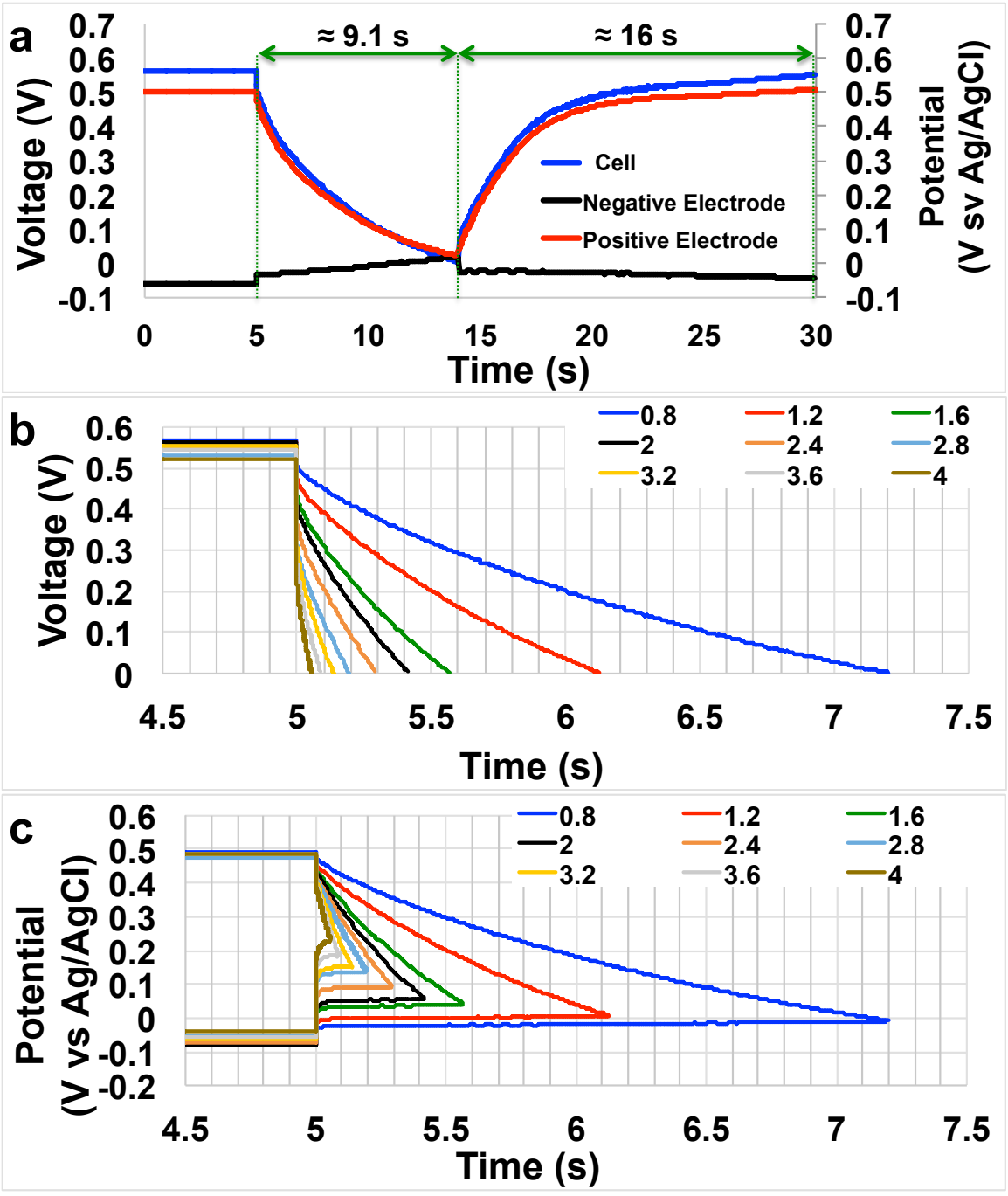
a
≈ 9.1 s
≈ 16 s
Voltage (V)
Potential (V sv Ag/AgCl)
Cell
Negative Electrode
Positive Electrode
Time (s)
b
Voltage (V)
0.8
1.2
1.6
2
2.4
2.8
3.2
3.6
4
Time (s)
c
Potential (V vs Ag/AgCl)
0.8
1.2
1.6
2
2.4
2.8
3.2
3.6
4
Time (s)

Figure 4

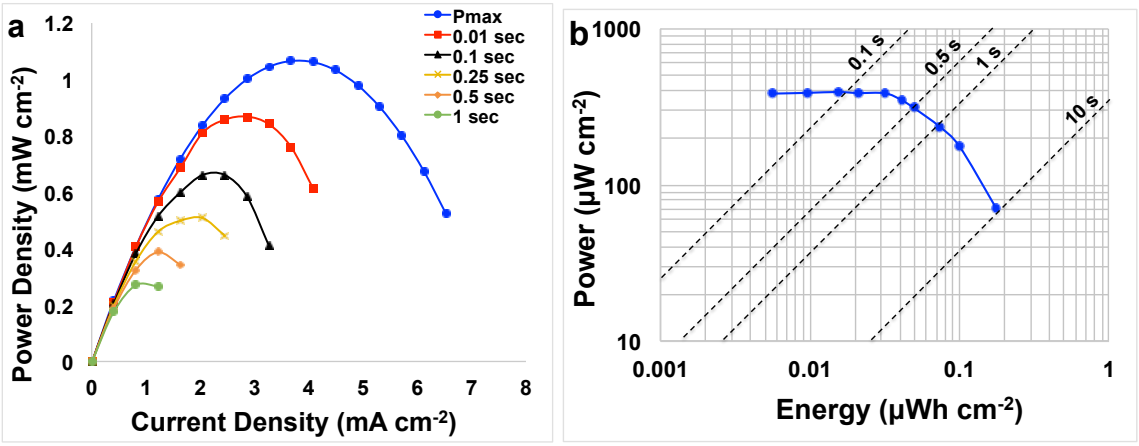
a
Power Density (mW cm-2)
Current Density (mA cm-2)
Pmax
0.01 sec
0.1 sec
0.25 sec
0.5 sec
1 sec
b
Power (μW cm-2)
Energy (μWh cm-2)
0.1 s
0.5 s
1 s
10 s